



**Sensitized Photon Upconversion in Anthracene-based
Zirconium Metal Organic Frameworks**

Journal:	<i>ChemComm</i>
Manuscript ID	CC-COM-03-2018-001893.R1
Article Type:	Communication

SCHOLARONE™
Manuscripts



Sensitized photon upconversion in anthracene-based zirconium metal-organic frameworks

J. M. Rowe^a, J. Zhu^a, E. M. Soderstrom^a, Wenqian Xu^b, Andrey Yakovenko^b, and A. J. Morris^{*a}

Received 00th January 20xx,
Accepted 00th January 20xx

DOI: 10.1039/x0xx00000x

www.rsc.org/

Sensitized upconversion is explored in three metal-organic frameworks (MOFs) constructed from the anthracene dicarboxylate (ADC) derivatives and zirconium nodes, 9,10-ADC (9,10-MOF), 2,6-ADC (2,6-MOF) and 1,4-ADC (1,4-MOF). Selective excitation of surface-bound Pd(II) mesoporphyrin IX (PdMP) gives rise to delayed fluorescence ($\tau = 370 \pm 30$ ns) from anthracene in the 9,10-MOF. The overall upconversion efficiency of the Pd@9,10-MOF is 0.46 ± 0.05 % with a threshold intensity of 104 ± 26 mW/cm².

Triplet-triplet annihilation-based upconversion (TTA-UC) is a process by which low energy photons are converted into higher energy photons.¹⁻³ Thus, TTA-UC has been proposed as a means to increase solar cell efficiency through the reduction of sub-bandgap spectral losses. First discovered by Parker in the 1960's, the potential application of TTA-UC in photovoltaics has attracted considerable attention from researchers in recent years and has been the topic of several review articles.³⁻⁷ The mechanism of TTA-UC involves sensitizer chromophores, which absorb lower-energy light and undergo intersystem crossing to the triplet state. An acceptor chromophore is then promoted directly to the triplet state via a Dexter-type electron exchange mechanism from the sensitizer. Two triplet excited state acceptors can interact and undergo TTA, resulting in a singlet state acceptor and fluorescence of higher-energy light. For many applications, including solar cell devices, solid-state upconversion systems are ideal. Solid-state upconversion systems typically involve suspension of the chromophores in soft-materials and glasses. However, this approach does not provide the ability to control molecular orientation and distance and as a result, these materials display greatly reduced

upconversion efficiencies compared to solution-based systems.^{8,9} That said, recent work by Hanson et. al. introduced a strategy for spatial control using self-assembled bilayers in which the donor and sensitizer molecules are linked together through a Zn(II) ion.¹⁰

Metal-organic frameworks (MOFs) provide an excellent platform for solid-state molecular upconversion. Their high surface area, rigid crystalline structure and porous nature provide a robust means of controlling molecular orientation, which can enhance molecular coupling, resulting in improved photophysical energy transfer processes. Additionally, the synthetic tunability of MOFs allows for the excitation and emission wavelengths to be altered by judicious choice of metal nodes and organic linkers. Furthermore, MOFs have demonstrated a proclivity for efficient photo-driven energy migration and reactivity.¹¹⁻¹⁸ The Kimizuka group first reported TTA-UC in a zinc MOF containing 9,10-dipyridyl anthracene (DPA) ligands, although the values of recorded efficiencies were later called into question.¹⁹ Later, Howard et al. demonstrated triplet energy transfer across heterojunctions of zinc MOFs from a Pd(II)porphyrin-containing sensitizer layer to a DPA-based emitter layers, followed by UC from the emitter layers.²⁰ In the current study, we systematically explore TTA-UC in three Zr MOFs constructed from three anthracene dicarboxylate (ADC) derivatives, 9,10-ADC (9,10-MOF), 2,6-ADC (2,6-MOF) and 1,4-ADC (1,4-MOF) in order to develop design rules for molecular and spatial orientation in MOFs. Zr-based MOFs are known to exhibit superior stability in comparison to Zn-carboxylate MOF structures and therefore, have greater potential for future device applications.

Anthracene and several of its derivatives have been utilized in TTA-UC systems in combination with a Pd porphyrin sensitizer.^{21,22} We recently described the photophysical properties of the three anthracene dicarboxylic acid derivatives listed above in dilute solutions.²³ Functionalization of anthracene with the electron-withdrawing carboxylate groups alters the excited-state properties of the parent molecule to various degrees depending on the location on the ring system. Therefore, we first

^a Department of Chemistry and Macromolecules Innovation Institute, Virginia Tech, Blacksburg, Virginia 24061, United States

^b X-ray Science Division, Advanced Photon Source, Argonne National Laboratory, Argonne, Illinois 60439, United States

† Electronic Supplementary Information (ESI) available: Experimental details, crystallographic models, UC emission spectra and time-resolved decay fits. See DOI: 10.1039/x0xx00000x

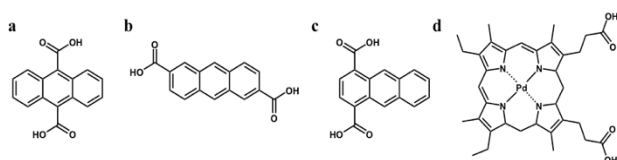


Fig. 1 Molecular structures of (a) 9,10-ADCA, (b) 2,6-ADCA, (c) 1,4-ADCA and (d) PdMP.

probed UC in DMF solutions of each ADCA ligand (1.0×10^{-3} M) and Pd(II) mesoporphyrin IX (PdMP, 1.0×10^{-11} M). Following 532 nm excitation, UC emission was observed from each anthracene derivative (Fig. S10-S15, ESI[†]). The lifetime of 9,10-ADCA increased from 4.20 ± 0.03 ns to 1.78 ± 0.01 μ s, from 9.0 ± 0.9 ns to 2.33 ± 0.03 μ s for 2,6-ADCA, and from 9.6 ± 0.1 ns to 1.60 ± 0.02 μ s for 1,4-ADCA.¹⁸ This substantial increase in the emission lifetimes is indicative of energy transfer (ENT) from the long-lived triplet excited state of PdMP. As a consequence of this Dexter-type ENT process, the emission lifetime of the sensitizer is considerably quenched. The quantum efficiency of energy transfer from the sensitizer to the acceptor (Φ_{ENT}) was estimated from the lifetimes of the sensitizer measured in the presence (τ) and absence ($\tau_0 = 19.5 \pm 0.8$ μ s) of the acceptor (Fig. S16-S18, ESI[†]). Using the equation $1 - \tau/\tau_0$, Φ_{ENT} was found to be ~ 90 %, 92 % and 84 % for the 9,10-ADCA, 2,6-ADCA and 1,4-ADCA samples, respectively. The quantum yield of UC (Φ_{UC} , equation 1) is given by the product of the quantum yield of intersystem crossing for the sensitizer (Φ_{ISC}), Φ_{ENT} , the yield of TTA (Φ_{TTA}) and acceptor fluorescence quantum yield (Φ_f).

$$\Phi_{UC} = \Phi_{ISC} \times \Phi_{ENT} \times \Phi_{TTA} \times \Phi_A \quad (1)$$

The UC quantum yields (Φ_{UC}) were determined experimentally using equation 2.²⁴

$$\Phi_{UC} = 2\Phi_{std} \left(\frac{A_{std}}{A_{UC}} \right) \left(\frac{F_{UC}}{F_{std}} \right) \left(\frac{I_{std}}{I_{UC}} \right) \left(\frac{\eta_{UC}}{\eta_{std}} \right)^2 \quad (2)$$

Here, A is the absorbance at the excitation wavelength, F is the integrated emission spectrum, I is the excitation intensity and η is the refractive index of the solvent.² The factor of 2 is added to adjust for the fact that two photons must be absorbed to generate one emitted photon. For 9,10-ADCA, 2,6-ADCA and 1,4-ADCA, Φ_{UC} were 1.21 %, 1.43 % and 1.08 %, respectively.

The three anthracene-containing ligands were incorporated into Zr-based MOFs and their propensity for photon UC was explored. We previously described the synthesis and photophysics of the 2,6-MOF and 1,4-MOF.²⁵ The 9,10-MOF was synthesized following a reported procedure.²⁶ The powder X-ray diffraction (PXRD) pattern of the 9,10-MOF (Fig. 2a) confirmed the formation of a crystalline material. As shown in the SEM images (Fig. 2b), the 9,10-MOF forms octahedral crystals ~ 1 μ m in size. Surface area measurements and thermal stability analysis are provided in the Supplemental Information. Although 9,10-MOF and UiO-66 are isostructural,²⁶ it is important to elucidate the MOF structure to determine the orientation, angle and distance between chromophores. The

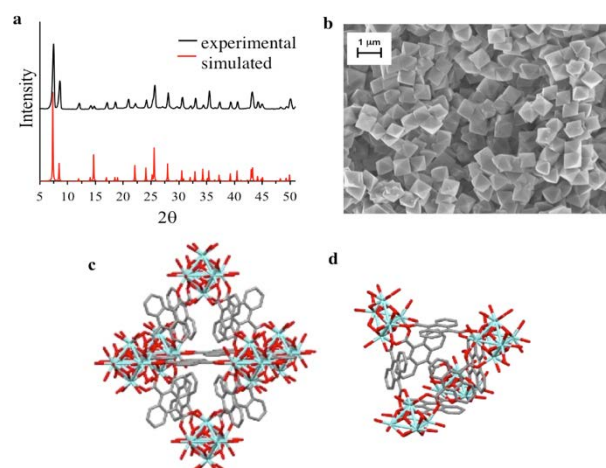


Fig. 2 (a) Experimental PXRD pattern of 9,10-MOF (black) compared with the simulated PXRD pattern (red), (b) SEM image of the 9,10-MOF and Wire-frame representation of the octahedral (c) and tetrahedral (d) cages of the 9,10-MOF crystal (c) the crystal structure.

crystal structure of the 9,10-MOF was determined by synchrotron powder X-ray diffraction (PXRD) at Advanced Photon Source (APS), Argonne National Laboratory (in Argonne, IL, USA). The 9,10-MOF forms a face centred cubic lattice in the space group Fm-3m with a lattice constant of 20.9073(1) \AA . The nearest distances between anthracene planes in the octahedral cage of the 9,10-MOF is 7.4 \AA . Crystallographic data for 9,10-MOF are summarized in Table S1. Further details about structure determination and refinement are summarized in the Supporting Information, Section 3.

The absorption and emission spectra of the 9,10-MOF are shown in Fig. 3. The excited-state properties of the 9,10-MOF are comparable to those of the fully protonated ligand.²³ The absorption spectrum of the 9,10-MOF exhibits substantial broadening of the vibronic bands and a large redshift of ~ 75 nm, relative to that of the free ligand. This is indicative of π - π interactions between the anthracene linkers in the ground state. The shape of the 9,10-MOF emission spectrum resembles that of 9,10-ADCA with some broadening of the tail emission. Likewise, both the fluorescence lifetime (Fig. S20, ESI[†]) and quantum yield of the 9,10-MOF ($\tau_A = 5.7 \pm 0.3$ ns, $\Phi_A = 0.3 \pm 0.1$) are similar to those measured for 9,10-ADCA ($\tau_A = 4.20 \pm 0.03$ ns, $\Phi_A = 0.29 \pm 0.06$).

The PdMP sensitizers were anchored to the surface of the MOFs by soaking the powder in a 0.5 mM PdMP/DMF solution

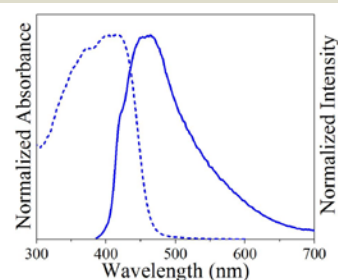


Fig. 3 Normalized absorption (dotted line) and emission (solid line) spectra of the 9,10-MOF, $\lambda_{ex} = 360$ nm.

Table 1. Photophysics of ADCA acceptors, PdMP sensitizer, and sensitizer-acceptor pairs

	Φ_A	τ_A (μ s)	τ_S	τ_{UC}	Φ_{ENT}	Φ_{UC}
9,10-ADCA	0.29 ± 0.06	4.20 ± 0.03	1.85 ± 0.03	1.78 ± 0.01	90.2 ± 0.2	1.21 ± 0.08
2,6-ADCA	0.32 ± 0.04	9.0 ± 0.9	1.73 ± 0.04	2.33 ± 0.03	91.6 ± 0.3	1.43 ± 0.08
1,4-ADCA	0.27 ± 0.03	9.6 ± 0.1	3.06 ± 0.05	1.60 ± 0.02	84.3 ± 0.3	1.08 ± 0.07
9,10-MOF	0.3 ± 0.1	5.7 ± 0.3	65.1 ± 0.1	0.37 ± 0.03	67.4 ± 0.6	0.46 ± 0.05
2,6-MOF	0.87 ± 0.04	16.6 ± 1.1	99.0 ± 0.3	-	50 ± 1	-
1,4-MOF	0.0020 ± 0.0001	$7.5 \pm 0.1; 19.9 \pm 0.1$	74.8 ± 0.3	-	63 ± 1.4	-

Φ_A = acceptor fluorescence quantum yield, τ_A = acceptor fluorescence lifetime, τ_{UC} = upconverted fluorescence lifetime, τ_S = sensitizer fluorescence lifetime in the presence of acceptor, Φ_{ENT} = energy transfer quantum efficiency, Φ_{UC} = upconversion quantum yield. Errors were calculated from measurements on three independent samples. It is important to note that the relative and absolute concentrations of both sensitizer and acceptor are critical to the reproducibility of the reported results (vide infra). All measurements were recorded on samples prepared with 1×10^{-11} M sensitizer and 1×10^{-3} M acceptor.

at 80 °C overnight. The MOFs were then washed several times with fresh DMF to remove excess or weakly associated PdMP. For spectroscopic studies, DMF suspensions of the PdMP@MOF powders (5 mg) were placed in a 24/40 jointed quartz cuvette, capped with a rubber septum, and purged with Ar for 1 hour. Upon 532 nm excitation, upconverted emission ($\lambda_{max} \sim 475$ nm) was clearly observed from the PdMP@9,10-MOF. However, no sensitized emission was detected from either the PdMP@2,6-MOF or PdMP@1,4-MOF samples measured under the same conditions. To confirm the stability of the MOF to the laser pulse, the sample was syringe filtered and the electronic absorption spectrum of the solution was recorded to ensure that no absorbance from the free ligand or sensitizer was observed.

The figures of merit (τ_A , Φ_{UC} , and I_{th}) for UC by PdMP@9,10-MOF were determined via time-resolved photoluminescence spectroscopy, Table 1. The lifetime of the upconverted emission from PdMP@9,10-MOF was $\tau_A \sim 370$ ns. The Φ_{ENT} was estimated to be $\sim 67\%$ (Fig. S16 and S22, ESI[†]). By employing equation 2, a Φ_{UC} of 0.46 % was calculated. To further confirm a TTA-based mechanism of UC in the PdMP@9,10-MOF, the UC emission was measured as a function of incident laser power (Fig. 4a). For a TTA-based UC mechanism, the UC emission intensity displays a quadratic dependence in the lower power region where the kinetics are limited by the triplet-state population and becomes linear at higher excitation power where TTA dominates the kinetics.²⁷⁻²⁹ The double logarithmic plot of the UC emission intensity of the 9,10-MOF as a function of excitation power density is shown in Fig. 4b. As anticipated, this plot yielded a slope of ~ 2 at low power density, indicative of a quadratic dependence, and a slope of ~ 1 at the highest power density. The threshold intensity (I_{th}) defines the intensity at which the triplet acceptor deactivation kinetics are driven by TTA.²⁹ I_{th} was determined from the intersection of the extrapolated slopes and the quadratic and linear dependences and was found to be 104.1 ± 26.4 mW/cm².

The reduced Φ_{UC} of the 9,10-MOF relative to the free ligand is likely due to the fact that the PdMP molecules are confined to the surface of the micron-sized MOF crystallites. The amount of PdMP in 5 mg of PdMP@9,10-MOF was determined by absorption spectroscopy (Fig. S7-S9, ESI[†]) and found to be $\sim 7 \times 10^{-10}$ mol and the amount of anthracene in the same sample was calculated to be $\sim 4 \times 10^{-6}$ mol (1×10^{-11} M and 1×10^{-3} M, respectively). For internal anthracene units to be active in the upconversion process, energy transfer between anthracene units must occur efficiently over large distances, ~ 500 nm. Long

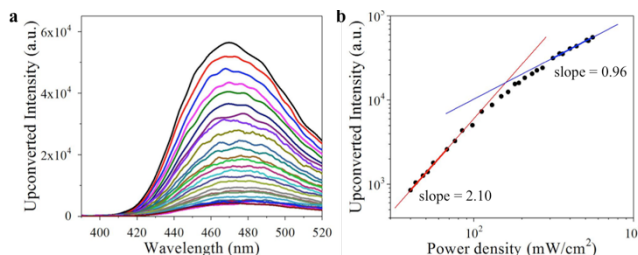


Fig. 4 (a) PdMP@9,10-MOF UC emission map, $\lambda_{ex} = 532$ nm (b) Excitation power dependence of UC emission intensity.

distance energy transfer has been observed in MOFs¹¹⁻¹⁸ and further studies into the energy transfer propensity of the MOFs presented herein are underway. If the interior anthracene units are not addressable, the measured Φ_{UC} represent a lower limit to the upconversion efficiency, as the anthracene concentration would be overestimated via the total absorbance of the MOF at the excitation wavelength. Thus, the Φ_{UC} could be improved by alternate synthetic methods, such as reducing the size of the MOF crystallites and/or introducing crystalline defects that allow for PdMP to be encapsulated in the interior of the MOF. Furthermore, Φ_{ENT} and Φ_{TTA} are proportional to chromophore (sensitizer and acceptor) concentrations and thus, optimization of these parameters could also improve the Φ_{UC} and decrease I_{th} .³⁰ Ideally, the concentration of the sensitizer should be increased to yield a higher concentration of excited acceptor molecules and increased probability for TTA-events. However, increased sensitizer could potentially lead to increased acceptor-to-donor back-ENT. Finally, optimization of the chromophore distances and orientations in the MOF could potentially enhance ENT processes and improve the overall Φ_{UC} . There is a clear decrease in Φ_{ENT} from the solution to the solid-state. The reduced degrees of freedom for the sensitizer bound at the MOF surface and resultant limitation to sensitizer/acceptor orientation, not surprisingly, negatively effects the efficiency of ENT at that interface. The effect of orientation in ENT may be the origin of the lower efficiency for 2,6-MOF compared to 9,10/1,4-MOF, which exhibit similarly oriented anthracene units.

Although all three ligands displayed UC emission in solution, only the 9,10-MOF comprises the appropriate distance (7.4 Å) and arrangement of anthracene moieties to enable ENT and TTA between the chromophores (Fig. 5a). Considering the structure of the 2,6-MOF, the distance and orientation of the anthracene moieties is not suitable for TTA (Fig. 5b). Because TTA is an electron exchange mechanism, there must be π -orbital overlap, which occurs at distances of < 10 Å. Refinements of the PXRD

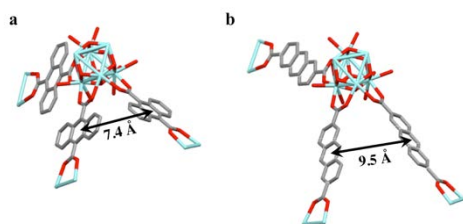


Fig. 5. Illustration of the spatial arrangement of anthracene moieties in the 9,10-MOF (a) and 2,6-MOF (b), based on the binding geometry of the ADCA ligands around the Zr₆O₄ nodes.

data for the 2,6-MOF revealed that this framework is isostructural with UiO-67 and has a lattice constant of 26.97 Å.²⁵ This corresponds to a distance of ~ 9.5 Å between anthracene planes within the MOF. Although the chromophores are within 10 Å, the orientation of the anthracene moieties at this distance does not provide sufficient orbital overlap to facilitate TTA. In contrast, coordination at the 1 and 4 positions of anthracene is presumed to result in much shorter distances between anthracenes within the 1,4-MOF, assuming a similar binding configuration at the Zr₆O₄ nodes. In this case, a larger portion of the aromatic plane likely occupies the pores of the 1,4-MOF.²⁵ Such arrangement allows for strong π - π interactions, which give rise to significant excimer formation. This is corroborated by the broad emission spectrum of the 1,4-MOF (~ 350 – 700 nm), along with a shorter lifetime component (7.5 ns) observed at 400 nm and a longer lifetime component (19.9 ns) at 550 nm.²⁵ In the 1,4-MOF, the process of excimer formation likely outcompetes ENT and TTA processes and is responsible for the absence of UC emission.

In summary, sensitized upconversion from a zirconium-based anthracenic MOF was demonstrated for the first time. Interestingly, systematic variation of the spacing between the acceptor anthracene units had dramatic effect on the upconversion efficiency. Specifically, only the 9,10-MOF demonstrated upconverted emission. The distance between anthracene linkers in the 2,6-MOF are too large for TTA to occur, while the short distances in the 1,4-MOF inhibit upconversion through competitive excimer formation. The results presented provide clear design rules with regard to three-dimensional structure and anthracene spacing to promote upconversion within MOFs. Methods to increase the efficiency of the process (concentration studies and further control over orbital and dipole overlap) are areas of continued investigation.

This material is based upon work supported by the U.S. Department of Energy, Office of Science, Office of Basic Energy Sciences under award number DE-SC0012446. This research used Beamline 17-BM at the Advanced Photon Source, a U.S. Department of Energy (DOE) Office of Science User Facility operated for the DOE Office of Science by Argonne National Laboratory under Contract No. DE-AC02-06CH11357.

Conflicts of interest

There are no conflicts to declare.

References

- 1 T. Trupke, M. A. Green and P. Würfel, *J. Appl. Phys.*, 2002, **92**, 4117-4122.
 - 2 T. N. Singh-Rachford and F. N. Castellano, *Coord. Chem. Rev.*, 2010, **254**, 2560-2573.
 - 3 T. F. Schulze and T. W. Schmidt, *Energy. Environ. Sci.*, 2015, **8**, 103-125.
 - 4 C. Duan, L. Liang, L. Li, R. Zhang and Z. P. Xu, *J. Mater. Chem. B*, 2018, **6**, 192-209.
 - 5 V. Gray, K. Moth-Poulsen, B. Albinsson and M. Abrahamsson, *Coord. Chem. Rev.*, 2018, **362**, 54-71.
 - 6 T. N. Singh-Rachford and F. N. Castellano, *Coord. Chem. Rev.*, 2010, **254**, 2560-2573.
 - 7 J. Zhao, W. Wu, J. Sun and S. Guo, *Chem. Soc. Rev.*, 2013, **42**, 5323-51.
 - 8 R. R. Islangulov, J. Lott, C. Weder and F. N. Castellano, *J. Am. Chem. Soc.*, 2007, **129**, 12652-12653.
 - 9 X. Jiang, X. Guo, J. Peng, D. Zhao and Y. Ma, *ACS Appl. Mater. Interfaces*, 2016, **8**, 11441-11449.
 - 10 S. P. Hill, T. Banerjee, T. Dilbeck and K. Hanson, *J. Phys. Chem. Lett.*, 2015, **6**, 4510-4517.
 - 11 C. A. Kent, D. Liu, T. J. Meyer and W. Lin, *J. Am. Chem. Soc.*, 2012, **134**, 3991-3994.
 - 12 C. A. Kent, B. P. Mehl, L. Ma, J. M. Papanikolas, T. J. Meyer and W. Lin, *J. Am. Chem. Soc.*, 2010, **132**, 12767-12769.
 - 13 C. Y. Lee, O. K. Farha, B. J. Hong, A. A. Sarjeant, S. T. Nguyen and J. T. Hupp, *J. Am. Chem. Soc.*, 2011, **133**, 15858-15861.
 - 14 J. Lin, X. Hu, P. Zhang, A. Van Rynbach, D. N. Beratan, C. A. Kent, B. P. Mehl, J. M. Papanikolas, T. J. Meyer, W. Lin, S. S. Skourtis and M. Constantinou, *J. Phys. Chem. C*, 2013, **117**, 22250-22259.
 - 15 W. A. Maza, R. Padilla and A. J. Morris, *J. Am. Chem. Soc.*, 2015, **137**, 8161-8168.
 - 16 H.-J. Son, S. Jin, S. Patwardhan, S. J. Wezenberg, N. C. Jeong, M. So, C. E. Wilmer, A. A. Sarjeant, G. C. Schatz, R. Q. Snurr, O. K. Farha, G. P. Wiederrecht and J. T. Hupp, *J. Am. Chem. Soc.*, 2013, **135**, 862-869.
 - 17 C. Wang and W. Lin, *J. Am. Chem. Soc.*, 2011, **133**, 4232-4235.
 - 18 W. A. Maza and A. J. Morris, *J. Phys. Chem. C*, 2014, **118**, 8803-8817.
 - 19 P. Mahato, A. Monguzzi, N. Yanai, T. Yamada and N. Kimizuka, *Nat. Mater.*, 2015, **14**, 924-930.
 - 20 M. Oldenburg, A. Turshatov, D. Busko, S. Wollgarten, M. Adams, N. Baroni, A. Welle, E. Redel, C. Wöll, B. S. Richards and I. A. Howard, *Adv. Mater.*, 2016, **28**, 8477-8482.
 - 21 F. Deng, J. Blumhoff and F. N. Castellano, *J. Phys. Chem. A*, 2013, **117**, 4412-4419.
 - 22 V. Gray, D. Dzebo, A. Lundin, J. Alborzpour, M. Abrahamsson, B. Albinsson and K. Moth-Poulsen, *J. Mater. Chem. C*, 2015, **3**, 11111-11121.
 - 23 J. M. Rowe, J. M. Hay, W. A. Maza, R. C. Chapleski, E. Soderstrom, D. Troya and A. J. Morris, *J. Photochem. Photobiol. A*, 2017, **337**, 207-215.
 - 24 G. A. Crosby and J. N. Demas, *J. Phys. Chem.*, 1971, **75**, 991-1024.
 - 25 J. M. Rowe, E. M. Soderstrom, J. Zhu, P. M. Usov and A. J. Morris, *Can. J. Chem.*, 2017, DOI: 10.1139/cjc-2017-0445.
 - 26 S. Pu, L. Xu, L. Sun and H. Du, *Inorg. Chem. Comm.*, 2015, **52**, 50-52.
 - 27 A. Haefele, J. Blumhoff, R. S. Khnayzer and F. N. Castellano, *J. Phys. Chem. Lett.*, 2012, **3**, 299-303.
 - 28 S. Jones, J. C. C. Atherton, M. R. J. Elsegood and W. Clegg, *Acta Cryst. C*, 2000, **56**, 881-883.
- A. Monguzzi, J. Mezyk, F. Scotognella, R. Tubino and F. Meinardi, *Phys. Rev. B*, 2008, **78**, 195112.